Soft Matter

PAPER

View Article Online
View Journal | View Issue

Cite this: *Soft Matter*, 2023, **19**, 2360

Environmentally responsive hydrogel composites for dynamic body thermoregulation†

M. Garzón Altamirano, [ab] M. G. Abebe, [c] N. Hergué, [a] J. Lejeune, [b] A. Cayla, [b] C. Campagne, [b] B. Maes, [c] E. Devaux, [b] J. Odent *[a] and J. M. Raquez [a]

Received 26th November 2022,
Accepted 25th February 2023

DOI: 10.1039/d2sm01548j

rsc.li/soft-matter-journal

Hydrogel composites exhibiting dynamic thermo-hydro responsive modulation of infrared radiation (IR) in the 5–15 μm range are designed for personalized body thermoregulation. Fabrication of the proposed system relies on the periodic arrangement of submicron-sized spherical fine silica (SiO_2) particles within poly(*N*-isopropylacrylamide) (PNIPAM)-based hydrogels. The dependence of the SiO_2 particles content on the IR reflection, followed by its modulation in response to any immediate environmental changes are thereby investigated. The addition of 20 wt% of SiO_2 allowed the hydrogel composites to reflect 20% of the IR emitted by the human body at constant temperature (*i.e.* T = 20 °C) and relative humidity (*i.e.* RH = 0%). According to Bragg's law, we found that the smaller the distance between the SiO_2 particles, the higher the IR reflection. The IR reflection further increased to a maximum of 42% when the resulting hydrogel composites are subjected to changes in relative humidity (*i.e.* RH = 60%) and temperature (*i.e.* T = 35 °C). Thermography is used to map the IR radiation emitted from the hydrogel composites when placed on the skin of the human body, demonstrating that the composite is actually reflecting IR. The latter results are supported by theoretical models that define the IR reflection profile of the resulting hydrogel composites with respect to the silica content, relative humidity and temperature.

A. Introduction

Thermoregulation refers to how the body maintains its internal temperature. Therein, controlling heat loss and gain is essential to provide users with better thermal comfort conditions.[1–3] Energy in the form of heat is transferred out of the human body by the skin through different transmission channel, *i.e.* conduction (5%), convection (15%), evaporation (20%) and radiation (60%).[4,5] Considering that the human body, at a normal skin temperature of *ca.* 34 °C, is emitting IR between 5 and 15 μm with a maximum emission wavelength at *ca.* 9 μm,[6–8] strategies used to manage thermal comfort recently focused on photonic structures.[9,10]

Photonic structures present periodic spatial variations of the effective refractive index, allowing them to propagate light waves at specific wavelengths defined by the length of the periodicity of the structure.[11,12] Thanks to their ability to interact with electromagnetic waves, photonic structures are nowadays widely used as displays, visible indicators and biological sensors.[12] Such ordered structures are herein typically composed of spontaneously arranged colloidal particle arrays embedded within polymer networks.[13] The distribution of colloidal particles within polymeric lattices acts as a natural diffraction grating for light waves when the interstitial spacing is on the same order of magnitude as the incident light wave.[12] Considering thermoregulation applications, fillers such as Ag,[5,9] Ni,[9] Zn/ZnO,[14] carbon nanotubes,[4] TiO_2 nanorods,[15] and Janus TiO_2–SiO_2 particles[16,17] have been used to increase the IR reflection. Thanks to their high density, stability, tightness and variable refractive index,[18,19] SiO_2 microspheres are also widely used to operate from ultraviolet (UV) to near-infrared (NIR) wavelengths.[20,21] As far as NIR are concerned, the submicrometric-sized SiO_2 microspheres are used as optical resonators randomly incorporated into a transparent polymer to enhance the reflection of infrared radiation.[6,22] Xiao *et al.*[6] therein demonstrated membranes based on polyamide nanofibres and submicron SiO_2 spheres with enhanced IR radiation. Similarly, Panwar *et al.*[16] coated cotton fabrics with Janus TiO_2–SiO_2 particles to enable clear NIR reflection due to the coupling of the high refractive index of TiO_2 and the large SiO_2 particles size.

Strategies to develop stimuli-responsive photonic materials that are able to modulate the IR radiation in response to

[a] *Laboratory of Polymeric and Composite Materials (LPCM), Center of Innovation and Research in Materials and Polymers (CIRMAP), University of Mons (UMONS), Mons, Belgium. E-mail: jeremy.odent@umons.ac.be*
[b] *University of Lille, ENSAIT, ULR 2461 - GEMTEX - Génie et Matériaux Textiles, F-59000 Lille, France*
[c] *Micro- and Nanophotonic Materials Group, Research Institute for Materials Science and Engineering, University of Mons, 20 Place du Parc, B-7000, Mons, Belgium*

† Electronic supplementary information (ESI) available. See DOI: https://doi.org/10.1039/d2sm01548j

various stimuli are being emerged.[23,24] Combining photonic structures with stimuli-responsive materials therein appeared as a promising way to achieve desired dynamic properties.[25,26] Hydrogels, *i.e.* three-dimensional polymer networks imbibed with aqueous solutions, are often invoked in such applications, given that they can reversibly change their volume or shape upon the trigger of different environmental stimuli.[27] In recent years, stimuli-responsive hydrogels such as poly(*N*-isopropylacrylamide) (PNIPAM), poly(ethylene glycol) diacrylate and polyacrylamide-*co*-acrylic acid have been increasingly used due to their versatility in the development of various types of photonic structures such as waveguides, photonic crystals, and fiber optics.[28] Among them, PNIPAM are of particular interest with respect to its lower critical solution temperature (LCST) at *ca.* 32 °C, *i.e.* close to the human body temperature.[29]

In the present study, the challenge of building stimuli-responsive hydrogels embedded with photonic crystals for the modulation of IR radiation at wavelengths around 5–15 μm is addressed. Fabrication of the proposed system relies on the incorporation of submicron-sized spherical fine SiO_2 particles and arranging them in a periodic structure within PNIPAM-based hydrogels. The dependence of the SiO_2 particles content on the IR reflection, followed by its modulation in response to any immediate environmental changes (*i.e.* relative humidity and temperature) are thereby investigated. The latter investigations are supported by theoretical models to provide the infrared radiation reflection profile of the resulting hydrogel composites upon the silica content, relative humidity and temperature.

B. Materials, design and characterization

Materials

N-Isopropylacrylamide (NIPAM, 97%, Sigma-Aldrich), acrylic acid (AA, 99.5%, Sigma-Aldrich). *N*,*N*′-Methylenebisacrylamide (MBA, 99%, Sigma-Aldrich), diphenyl(2,4,6-trimethylbenzoyl) phosphine oxide (TPO, 97%, Sigma-Aldrich) and methanol (99.8%, VWR) are used without any further purification. Monodispersed spherical silica particles with an average particle size of 100 nm and a density of 2.21 g cm^{-3} (Fuji Chemical, Silibol 100) are used. Deionized water was obtained with a Milli-Q system (Millipore).

Design of PNIPAM-based hydrogel composites

PNIPAM-based hydrogel composites are synthesized by free radical photo-polymerization using NIPAM as monomer, AA as co-monomer, MBA as crosslinker, and TPO as photoinitiator in the presence of submicron-sized spherical fine SiO_2 particles with a uniform size of 100 nm. For this purpose, 2 g of NIPAM, 0.038 g of MBA (2 mol%), 0.064 g of AA (5 mol%), and various amounts of SiO_2 (from 0 to 40 wt%) are dissolved in 4 mL of a 75 : 25 vol% methanol : water mixture. Afterwards, the final addition of 0.026 g of TPO (0.5 mol%) enables the free radical photo-polymerization of the acrylate groups with near-UV exposure (2000 W cm^{-2}) for 30 seconds. Therein, a Petri mold of 3 cm of diameter is used to cast the different dissolutions in order to obtain the same thickness (*i.e.* 2 mm) for all the hydrogel composites after the photo-polymerization. The resulting hydrogel composites are subsequently washed for at least 24 h in the 75 : 25 vol% methanol : water mixture before drying them at 50 °C under vacuum up to constant weight.

Characterization

Gel fraction. The gel fraction (%GF) is determined according to eqn (1).[30] The resulting hydrogel composites are thereby dried at 50 °C under vacuum up to constant weight and weighed (W_1). The materials are subsequently immersed at least 24 h in the 75 : 25 vol% methanol : water mixture to remove any unreacted reagents and dried again at 50 °C under vacuum up to constant weight and weighed (W_2).

$$\%\mathrm{GF} = \frac{W_2}{W_1} \times 100 \quad (1)$$

Swelling ratio. The swelling ratio (%S) is determined according to eqn (2). The resulting hydrogel composites are dried at 50 °C under vacuum up to constant weight and weighed (W_1). The materials are subsequently soaked in distilled water and weighed (W_s) at specific time intervals until the equilibrium swelling is reached.

$$\%S = \frac{W_s - W_1}{W_1} \times 100 \quad (2)$$

LCST determination. Differential Scanning Calorimetry (DSC, TA instruments) is conducted using heat/cool/heat analysis from 20 °C to 50 °C with a scan rate of 3 °C min^{-1} under nitrogen atmosphere to determine the LCST of PNIPAM-based hydrogels. For this purpose, *ca.* 5–10 mg of previously swollen (*i.e.* at equilibrium swelling state) hydrogels are encapsulated in an aluminum hermetic pan while distilled water is introduced into the reference pan. The LCST point is recorded from the first endothermic peak of the second heating cycle.

Fourier transform infrared spectroscopy. A Shimadzu IR Prestige-21 spectrometer equipped with an integrating sphere is used in reflectance mode from 2 μm (5000 cm^{-1}) to 28 μm (350 cm^{-1}). The experimental data are collected and analyzed using the Varian Resolutions Pro software. As far as humidity cycles are concerned, the hydrogel composites are subjected to changes in relative humidity (from *ca.* 0%RH to 90%RH) within a climate chamber (Memmert 605-02) at constant temperature (20 °C). The samples are therein kept for one hour at the targeted relative humidity to reach the equilibrium of the system. Typical humidity cycle begin with the dried materials (*i.e. ca.* 0%RH), then the relative humidity is gradually increased to 45, 60, 75, and 90%RH, followed by the gradual decrease up to 45%RH to complete the cycle. Each humidity cycle is performed at least three times. Concerning the temperature testing, the hydrogel composites are subjected to changes in temperature within a climatic chamber (Memmert

605-02) at constant relative humidity (*i.e.* 60%RH). The samples are therein kept for one hour at the targeted temperature to ensure the equilibrium of the system. Typical temperature tests begin at 20 °C, then the temperature is gradually increased to 30 °C, 35 °C, 40 °C and 50 °C. The errors do not exceed 1.5 °C during the temperature testing.

Scanning electron microscopy. A Hitachi SU8020 device at a voltage of 5 kV is used to record the morphology and related distribution of the SiO_2 particles within the hydrogel composites. The dried materials are cut into small pieces, soaked into distilled water up to constant weight (*i.e.* at equilibrium swelling state), and then freeze-dried to maintain their three-dimensional structure and observe their porosity. The changes on the surface of hydrogels composite at the different relative humidity and temperature are recorded using pre-equilibrated, freeze-dried, materials in their respective surrounding environmental conditions. The resulting materials are coated with thin layer of carbon as conductive material to obtain high-quality images. Analysis software ImageJ is used for the analysis of SEM images to estimate the particles size and their distribution within the matrix.

Roughness. Roughness is recorded with a Bruker DektakXT profilometer using pre-equilibrated, freeze-dried, materials at the different humidity and temperature conditions. As a result, roughness parameters, *i.e.* R_a (the mean value of the deviations of the surface height) and R_q (root-mean-square value of the departures of the profile) are obtained and averaged from at least five measurements. In addition, 3D roughness analysis is performed by constructing a 1 mm^2 surface mapping using a 2 μm tip (500 lines per surface at 10 s per line).

Thermal imaging. A FLIR C2 compact professional thermal imaging camera (80 × 60 pixels) is used to record any infrared radiation in a spectral range of 7.5–14 μm and a temperature range of −10 to 150 °C with an image upgrade rate of 9 Hz. The materials are kept under constant relative humidity and temperature conditions (*i.e.* 60%RH and 20 °C) and placed 15 s on the skin to get the thermal equilibrium prior to imaging. Thermal images are captured at a fixed distance of 10 cm.

Theoretical model. The modeling framework consists of electromagnetic, radiative transfer, and thermal analysis steps. First, the optical properties of a single silica particle is investigated using an electromagnetic model (solving the scattering problem). Then, the effective radiative properties of a particle cloud uniformly dispersed in a polymer matrix is obtained using incoherent summation rules. The collision-based Monte Carlo (MC) method is finally used for solving the radiative transfer through the materials, allowing to retrieve the spectral reflectance. The finite element method is also used to calculate rigorous solutions of Maxwell's equations using commercial software (COMSOL Multiphysics® v5.3). Once we have the spectral reflectance, the integrated reflectance is calculated using the human body emission spectrum and modeled using Planck's distribution, assuming that it is a black body at a skin temperature of 34 °C.[9,10] Finally, we utilized the integrated reflectance in a heat balance analysis to study thermal transport through the fabric, leading to the ambient setpoint temperature. A thermal circuit-based 1D steady-state heat transfer model is used to understand the heat transfer process from the human body through the fabric to the ambient.

C. Results and discussion

Hydrogel composites exhibiting dynamic thermo-hydro responsive modulation of infrared reflection for personalized body thermoregulation are designed. Adding submicron-sized spherical fine silica particles and arranging them in a periodic structure within PNIPAM-based hydrogels is herein envisioned as a simple and versatile strategy to tune the infrared reflection in response to any immediate environmental changes. These proposed hydrogel composites are fabricated upon a free-radical copolymerization of NIPAM with acrylic acid (AA) co-monomers in the presence of *N*,*N*′-methylenebisacrylamide (MBA) as crosslinker. Diphenyl(2,4,6-trimethylbenzoyl) phosphine oxide (TPO), a type-I photo-initiator, enables the free radical photo-polymerization of the acrylate groups within 30 s under near-UV exposure. Herein, the LCST of PNIPAM-based hydrogels is adjusted more precisely to human body temperature by the simple addition of 5 mol% of AA. Further adding submicron-sized spherial silica (SiO_2) particles of a uniform size of 100 nm within the crosslinked polymer networks endow the final materials with photonic properties. The fine monodisperse SiO_2 particles spontaneously formed colloidal particle arrays in a nonclosest-packed state, leading to Bragg reflection as-generated by the spacing between the diffracting planes of the colloidal crystals.[31] The dependence of the SiO_2 particles content on the physicochemical properties of the resulting hydrogel composites are thereby investigated. At first, we found that the gel fractions, which are above 90%, are not affected by the addition of silica particles (Table S1, ESI†). The latter results highlight our ability to rapidly (*i.e.* within 30 s) reach a high degree of conversion through the use of a near-UV source. Although the LCST remains within the skin temperature range (33.5–37 °C), the LCST of the thermoresponsive PNIPAM-based hydrogels slightly decrease upon the addition of SiO_2 particles (Table S1, ESI†). Finally, the swelling ability of the resulting hydrogel composites also decreases with the addition of SiO_2 particles (Table S1, ESI†). This behavior is attributed to the temporary crosslinks provided by the SiO_2 particles within the hydrogel networks, providing localized region of enhanced strength.[32] The morphology of the hydrogel composites is further investigated by scanning electron microscopy, showing homogeneously distributed SiO_2 within the hydrogel composites up to 20 wt%. Likewise, the distance between the dispersed SiO_2 particles within the hydrogel decreases with the SiO_2 loading (Fig. S1, ESI†). At higher SiO_2 loadings (*i.e.* >20 wt%), the formation of aggregates is observed (Fig. S2, ESI†), leading to higher distance between the SiO_2 particles (Fig. S2, ESI†).

To demonstrate the ability of the hydrogel composites to reflect light in the mid-far infrared range (5–15 μm) in the frame of body thermoregulation, near-infrared reflectance spectroscopy is used with respect to the silica content, relative

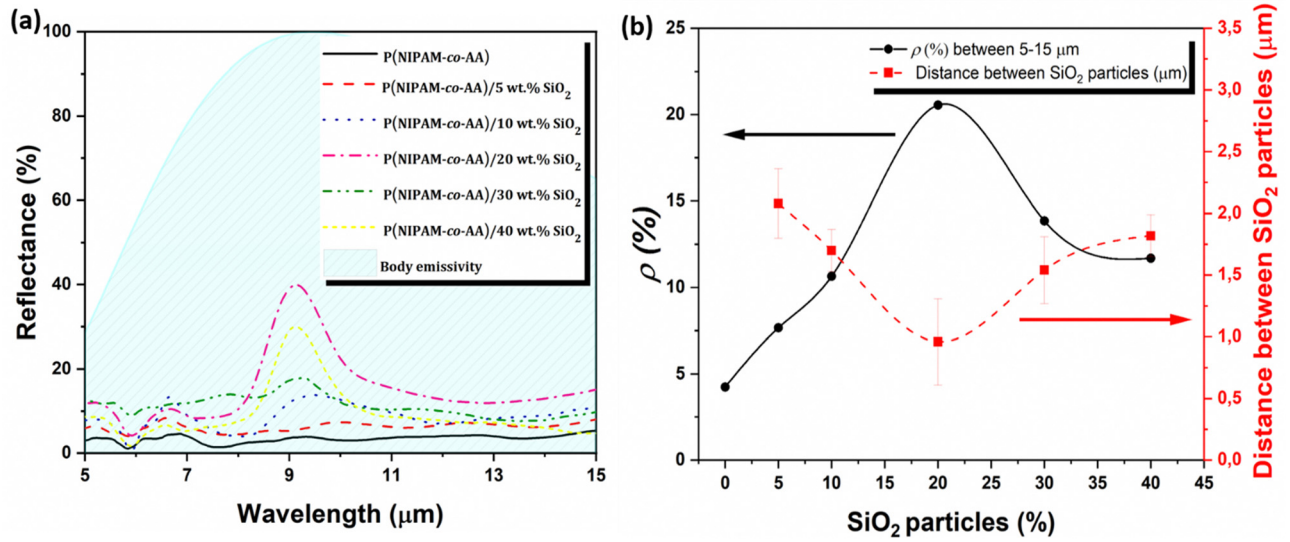

Fig. 1 (a) Evolution of the reflectance in the 5–15 μm range of the PNIPAM-based hydrogel composites as a function of the SiO_2 content, with the human body emissivity at a skin temperature of 34 °C. (b) Percentage of infrared radiation emitted by the human body that is reflected by the PNIPAM-based hydrogel composites (black circles) as well as the distance between the SiO_2 particles (red squares) with respect to the SiO_2 content.

humidity and temperature. The near-infrared reflectance spectra revealed a dependence of the silica content at wavelengths around 6–7 μm and 9 μm (Fig. 1a). At 6–7 μm wavelength, the reflectance varies between 6 and 12% in intensity, which is ascribed to the backscattering of some photons (*i.e.* electromagnetic waves) within the hydrogel composites.[33] In contrast, the reflectance around 9 μm is attributed to the bulk reflection of the hydrogel composites as well as the characteristic reflection peak of silica due to its high refractive index at this wavelength.[34] Therein, the hydrogels composites loaded with 20 wt% SiO_2 reached the maximum intensity at 9 μm with 40% of reflectance, corresponding to the reflection of 20% of the human body emission (Fig. 1b). The dependence of the SiO_2 particles content on the reflectance at 9 μm probably arise from the bulk density of SiO_2 that linearly affects the refractive index of the hydrogel matrix. As a result, a larger refractive index difference between the propagating media (the hydrogel composite from one side and air from the other side) produces a stronger reflection of the radiation at bulk interaction level.[35] $\rho(\%)$ is determined as a standard measure of the percentage of infrared radiation emitted by the human body that is reflected by the hydrogel composite using eqn (3),

$$\rho(\%) = \frac{\int_{\lambda_1}^{\lambda_2} R(\lambda)\phi_{bb}(\lambda)d\lambda}{\int_{\lambda_1}^{\lambda_2} \phi_{bb}(\lambda)d\lambda} \times 100 \quad (3)$$

where $R(\lambda)$ is the reflection spectrum of each sample, ϕ_{bb} is Planck's black body distribution for a skin temperature at 34 °C, and (λ_1, λ_2) is the wavelength interval of the human body thermal emission spectrum (*i.e.* 5–15 μm) (Table S2, ESI†). Fig. 2b shows the total percentage of infrared radiation reflected by the hydrogel composites as a function of the SiO_2 particles content. It is observed that the reflection increases upon the addition of silica up to 20 wt% SiO_2. However, higher concentrations (*i.e.* 30–40 wt%) lead to a decrease of the percentage of reflected infrared radiation due to an alteration in the dispersion of the SiO_2 particles (see Fig. S1, ESI†). According to Bragg's law,[31,36] the reflection of infrared radiation is affected by the amount and distribution of SiO_2 particles within the hydrogel matrix. Therefore, the lower the SiO_2 content, the higher the distance between the distributed particles and the lower the IR reflection. At higher the SiO_2content, the smaller the distance between the particles and the higher the IR reflection percentage. However, the formation of agglomeration at high SiO_2 contents causes the distance to increase and the IR reflection to decrease. According to the results, the distance between the particles is minimized at 20 wt% SiO_2 (Fig. S2, ESI†), reaching the maximum percentage of reflected infrared radiation.

The thermo-hydro responsive modulation of infrared reflection using the hydrogel composites containing 20 wt% of silica is subsequently investigated. We found that the reflectance intensity at 9 μm change at constant temperature (*i.e.* 20 °C) with respect to the relative humidity (Fig. 2a). As a result, the reflectance intensity increases from 0%RH to 60%RH, and subsequently decrease at higher relative humidity, *i.e.* up to 90%RH. The percentage of reflected infrared radiation within the 5–15 μm range, *i.e.* ρ, is further determined with respect to the relative humidity (Fig. 2b and Table S2, ESI†).

Recall that the hydrogel composites reflect *ca.* 20% of the infrared radiation emitted by the human body at 0%RH and 20 °C. At higher relative humidity, ρ increase from *ca.* 20% to 30% at 60%RH, then decrease up to *ca.* 17% at 90%RH. PNIPAM-based hydrogels can reversibly change their volume or shape upon the trigger of environmental stimuli such as temperature and relative humidity.[37,38] Under the different relative humidities, the hydrogels composites swell until reaching its equilibrium state (Fig. S3, ESI†). While the swelling

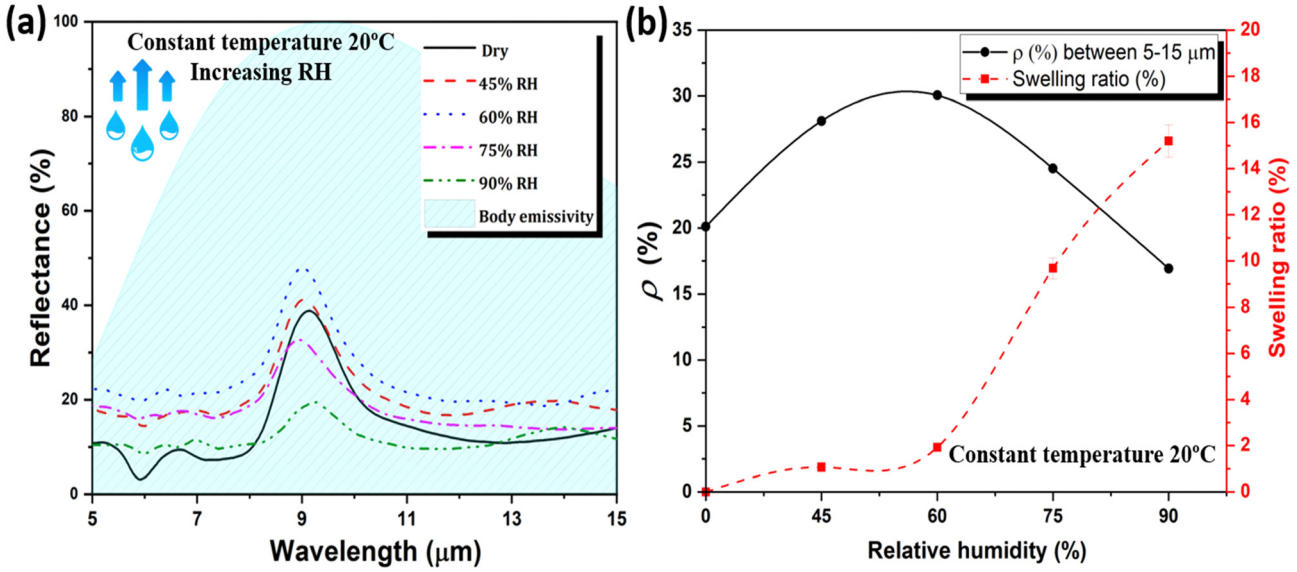

Fig. 2 (a) Evolution of the reflectance in the 5–15 μm range of the PNIPAM-based hydrogel composite containing 20 wt% of SiO_2 as a function of the relative humidity at constant temperature of 20 °C, with the human body emissivity at a skin temperature of 34 °C. (b) Percentage of infrared radiation emitted by the human body that is reflected by the PNIPAM-based hydrogel composite containing 20 wt% of SiO_2 (black circles) as well as the swelling ratio (red squares) with respect to the relative humidity.

index of the hydrogel composites are not exceeding 2% below 60%RH, the swelling index significantly increase at higher relative humidities, reaching *ca.* 15% at 90%RH (Fig. 2b). Therein, the higher the swelling index, the higher the volume change of the hydrogel matrix and the higher the distance between the SiO_2 particles within the hydrogel matrix (Fig. S4 and S5, ESI†). As a result, higher relative humidity than 60%RH leads to lower Bragg's reflection as shown in Fig. 2b.[31,39] By contrast, below 60%RH, the volume change is not significant enough to abruptly affect the distance between the SiO_2 particles (Fig. 3), so that the bulk Bragg reflection cannot rationalize the recorded reflectance. Still, the Bragg reflection is found to be also critically dependent on the surface morphology (Fig. S6, ESI†).[40,41] The low swelling index (*i.e.* <2%) recorded at relative humidities below 60%RH is affecting the surface morphology of the resulting hydrogel composites (Fig. 3 and Table S3, ESI†). While the hydrogel composites have a tight, dense, rough and wavy surface at 0%RH, a progressive decrease in surface roughness is observed as the relative humidity increases (Fig. 3). As a result, the reflection of radiation at surface level increases when the roughness of the hydrogel composites decreases.

Overall, the bulk Bragg reflection thereby dominates at high relative humidities (*i.e.* >60%RH), while the surface Bragg reflection dominates at low relative humidities (*i.e.* <60%RH). The latter result is consistent with the increase of ρ from 0%RH to 60%RH with respect to a decrease of the surface roughness, followed by a decrease of ρ from 60%RH to 90%RH with respect to an increase of the particles distance within the hydrogel matrix (Fig. 3). Applying relative humidity cycling ultimately attest for the reversible modulation of the infrared reflection with respect to the relative humidity (Fig. S7, ESI†). As far as constant relative humidity is concerned

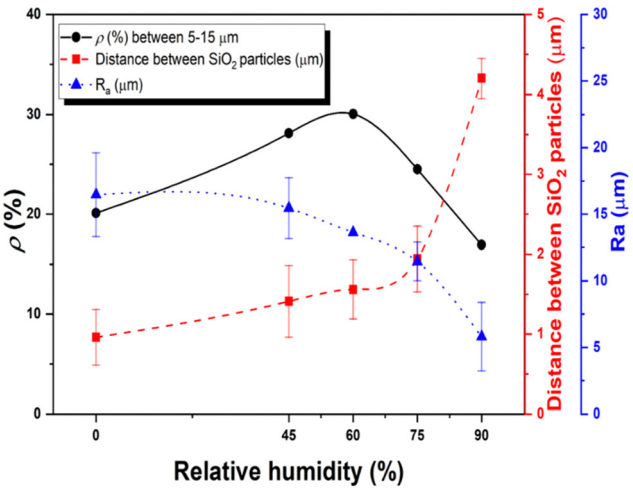

Fig. 3 Relationship between the percentage of infrared radiation emitted by the human body that is reflected by the PNIPAM-based hydrogel composite containing 20 wt% of SiO_2 (black circles), the distance between the SiO_2 particles (red squares) and the surface roughness (blue triangles) with respect to the relative humidity.

(*i.e.* 60%RH), we found that the reflectance intensity at 9 μm also change with respect to the applied temperature (Fig. 4a). The reflectance intensity increases from 50% at 20 °C to 80% at 35 °C, then decreases to 20% at 50 °C. ρ is further determined with respect to the temperature (Fig. 4b and Table S2, ESI†), reflecting *ca.* 30% of the infrared radiation emitted by the human body at 20 °C and 60%RH. At higher temperature, ρ increase from *ca.* 30% to 42% at 35 °C, then decrease up to *ca.* 26% at 50 °C. Although the swelling index of the PNIPAM-based hydrogel composites are not exceeding 2.5% during the temperature

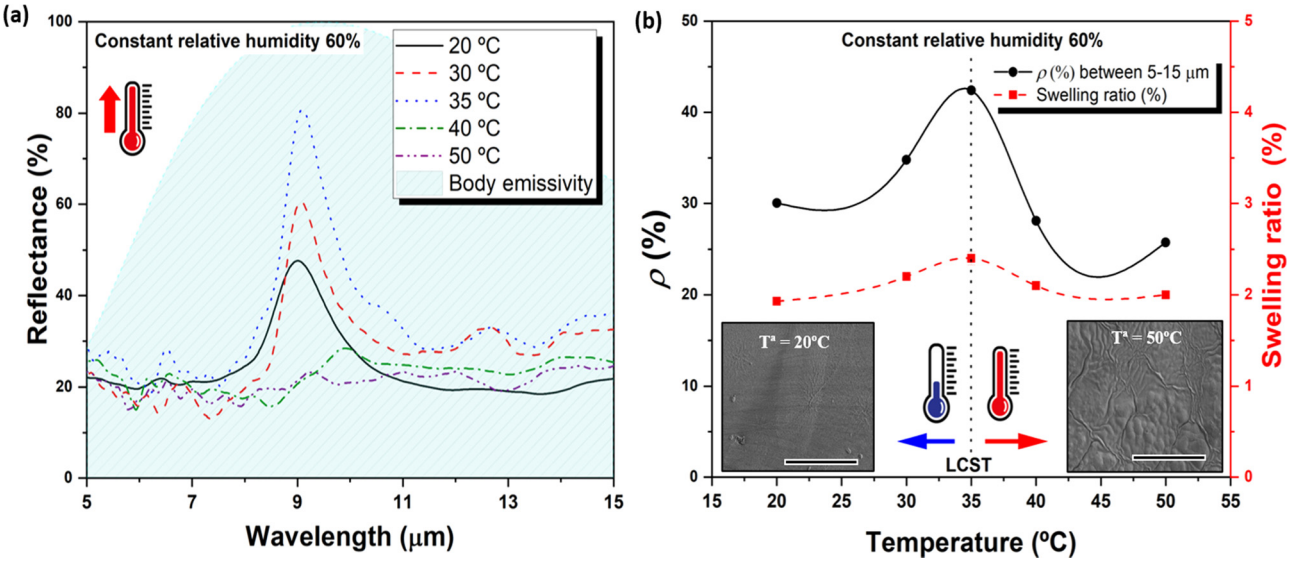

Fig. 4 (a) Evolution of the reflectance in the 5–15 μm range of the PNIPAM-based hydrogel composite containing 20 wt% of SiO_2 as a function of the temperature at constant relative humidity of 60%, with the human body emissivity at a skin temperature of 34 °C. (b) Percentage of infrared radiation emitted by the human body that is reflected by the PNIPAM-based hydrogel composite containing 20 wt% of SiO_2 (black circles) as well as the swelling ratio (red squares) with respect to the temperature.

testing, thus limiting the temperature-induced shrinking of the overall materials, the results are consistent with the phase transition of the PNIPAM-based hydrogel composites above its lower critical solution temperature (LCST at *ca.* 35 °C).[42] The subsequent release of entrapped water molecules from the swollen PNIPAM-based hydrogel network when placed above the LCST results in significant volume reduction, thus affecting the Bragg reflection with respect to change in the particles distance within the hydrogel matrix (Fig. S8 and S9, ESI†) as well as in the surface roughness (Table S4 and Fig. S10, ESI†). While the particles distance within the hydrogel matrix does not seem to be significantly affected by the temperature, the surface roughness is found to be critically dependent on the temperature (Fig. 5). Below its LCST, the surface roughness decreases from 15 μm at 20 °C to 10 μm at 35 °C with respect to its softening at higher temperature as the hydrogel composite is slightly swollen. Above its LCST, the whole material volume contract caused by the shrinkage of the thermoresponsive PNIPAM-based hydrogels,[43] leading to higher surface roughness.[44] The dependence of the temperature on the reflectance is thereby dominates by the surface Bragg reflection, rather than the bulk Bragg reflection (Fig. 5).

As a proof-of-concept demonstration, infrared thermography is used to map the infrared radiation emitted from the hydrogel composites when placed on the skin of the human body, providing the apparent surface temperature of the materials (Fig. 6). Radiation emitted by the human body can be absorbed, transmitted or reflected by the hydrogel composites in contact with the skin. While absorbed or transmitted radiation would show apparent "warm" temperatures, equal to, or greater than the skin temperature, reflected radiation would show "cold" apparent temperatures since the infrared radiation is returning to the emission focus. Therein, the thermal images show a "warm" apparent temperature (*i.e.* 32.9 °C) for

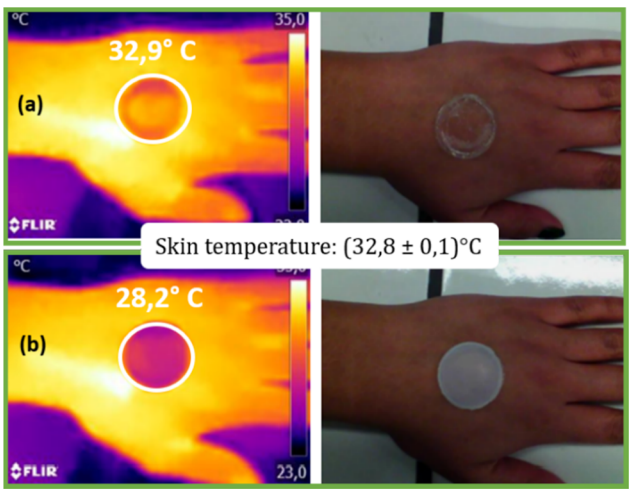

Fig. 5 Relationship between the percentage of infrared radiation emitted by the human body that is reflected by the PNIPAM-based hydrogel composite containing 20 wt% of SiO_2 (black circles), the distance between the SiO_2 particles (red squares) and the surface roughness (blue triangles) with respect to the temperature.

the neat PNIPAM-based hydrogels, suggesting that the neat material is absorbing or transmitting rather than reflecting the infrared radiation. In contrast, the hydrogel composites show a "cold" apparent temperature (*i.e.* 28.2 °C), demonstrating that the composite is actually reflecting infrared radiation.

D. Theoretical models

Theoretical models are designed to support the infrared radiation reflection profile of the hydrogel composites upon the silica content, relative humidity and temperature. For the

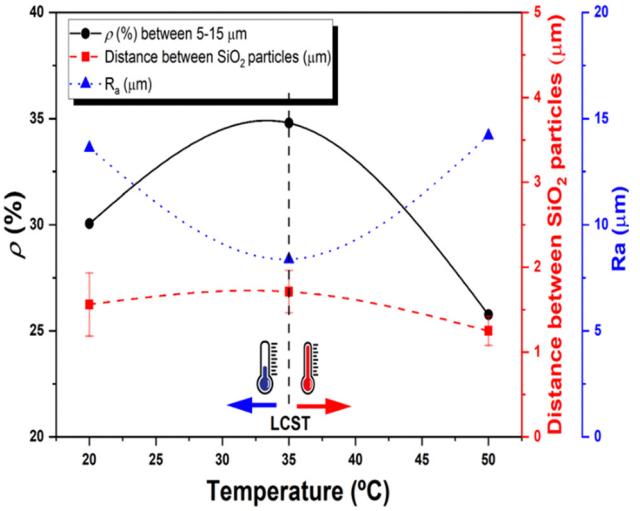

Fig. 6 Infrared thermography images (left) and real images (right) of (a) the neat PNIPAM-based hydrogel and (b) the PNIPAM-based hydrogel composite containing 20 wt% of SiO_2. Thickness: 2 mm; relative humidity: 60%; temperature: 20 °C.

realization of the theoretical models, the hydrogel matrix is assumed to be an ideal polymer whose refractive index is set to 1.5 as an approximate value for PNIPAM-based materials.[45] In addition, it is assumed that the hydrogel matrix does not absorb infrared radiation with an extinction coefficient of zero. It was further assumed that the particles are homogeneous and uniformly dispersed within the resulting hydrogel composites while the refractive index and extinction coefficient of silica are taken from the results published by J. Kischkat *et al.*[46] First, the reflection of infrared radiation is investigated as a function of the addition of SiO_2 particles within the hydrogel matrix (Fig. 7a). PNIPAM-based hydrogel does not show any reflection intensity peaks in the wavelengths range of 5–15 μm. Upon the addition of silica within the PNIPAM-based hydrogels, the reflection peak around is due to the fact that silica has a strong phonon-polariton resonance at this wavelength. At this wavelength, silica has a large extinction coefficient (k), thus a negative permittivity. Consequently, there will be a large impedance mismatch between air and silica to give a significant reflection.[47] The intensity of this peak depends on the amount of silica dispersed within the hydrogel matrix since the reflection of the infrared radiation is governed by the bulk interaction, *i.e.* by the distribution of SiO_2 particles within the matrix.

In order to analyze the influence of the interaction at the bulk level, hydrogel composites with 20 wt% of SiO_2 are used while the reflection of infrared radiation in the wavelength's range of 5–15 μm is simulated as a function of water content, assuming a flat surface. The water content (wt%) is obtained experimentally at different relative humidities and used for the simulations (Fig. S3, ESI†). The hydrogel composites swell depending on the humidity conditions, so that its volume increases with respect to the water content (Fig. S11a, ESI†). The Monte Carlo simulation shows the reflection profiles on the infrared radiation as a function of the water content (Fig. 7b). As a result, the intensity of the reflection peak at 9 μm slightly decreases with respect to the water content. This is because the change in the matrix volume changes the distance between the SiO_2 particles dispersed within the hydrogel matrix. Increasing the particles distance decreases the bulk reflection. The interaction at the surface level is investigated using the hydrogel composites with 20 wt% SiO_2 and simulating the reflection of infrared radiation in the range of 5–15 μm as a function of the change in surface morphology, assuming no change in volume. A completely flat surface and a completely wrinkled surface are simulated to discuss the effect of the surface on the reflection of infrared radiation (Fig. S11b, ESI†). As obtained by finite element method using COMSOL, the flat surface presents a more intense infrared reflection profile, highlighting the high intensity of the reflection peak around 9.7 μm (Fig. 7c). The latter is due to the presence of silica particles on the surface, acting as a thin film and therefore reflecting more infrared radiation.[46,48] The wrinkled surface has a discrete refraction profile in which the characteristic peak of SiO_2 is not observed since the effect of the surface on the reflection of infrared radiation has more influence, so that the reflection of infrared radiation is dominated by the surface morphology. The results published by Gorodetsky *et al.*[41] confirmed this behavior by developing adaptive infrared reflection structures based on a wrinkled structure. One can conclude that the simulated theoretical models correspond to the experimental results obtained as the behavior of the designed hydrogel composites is in accordance with the theoretical models.

Finally, the thermal efficiency of the hydrogel composites is evaluated in order to determine the maximum and minimum temperatures that the material can maintain without affecting the thermal comfort of the user (*i.e.* ambient setpoint temperature) (Fig. 7d). This temperature range is defined by assuming a constant body heat generation of Q = 70 W m^{-2},[49] corresponding to a sedentary individual with a skin temperature of 34 °C. Therefore, the equality between body heat generation and the sum of radiative, conductive and convective heat fluxes defines the thermal comfort of the user. A typical air gap of 1 mm is also assumed for the microclimate thickness. Furthermore, the thermal conductivity of air is k_{air} = 0.03 W m^{-1} K^{-1}, the natural convective heat transfer coefficient is h = 3 W m^{-2} K^{-1},[49] the thickness of the hydrogel composites is 2 mm, the emissivity of the skin is approximated as gray body with ε_{skin} = 0.98, the emissivity of the ambient environment is approximated as a black body with ε_{amb} = 1. Fig. 7d shows the evolution of the set point ambient temperature required to reach the comfort skin temperature of T_s = 34 °C as a function of the infrared radiation reflected by the hydrogel composites. The set point temperature decreases as the percentage of reflected infrared radiation (*i.e.* ρ) increases. In the absence of silica particles, the neat hydrogel matrix reflects 5% of the infrared radiation emitted by the human body (Fig. 1b). With this percentage of reflection, the environmental temperature at which the hydrogel could be used while maintaining the thermal comfort of the individual should be 25.7 °C. With the

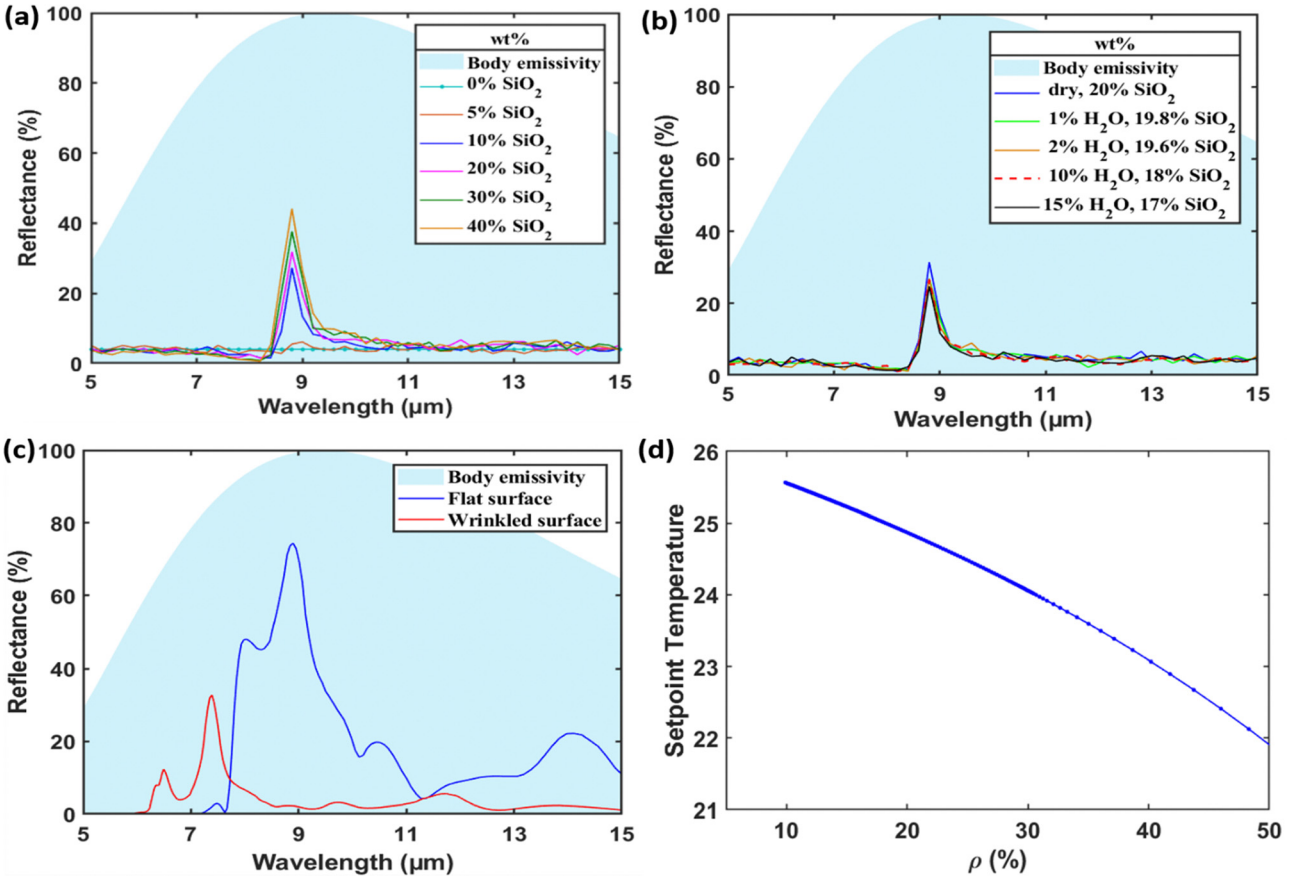

Fig. 7 Theoretical models obtained from the experimental data supporting the infrared radiation reflection profile of the PNIPAM-based hydrogel composites upon (a) the silica content, (b) the relative humidity with respect to the water content within the hydrogel composite, and (c) the temperature with respect to flat and wrinkled surfaces, with the human body emissivity at a skin temperature of 34 °C. (d) Evolution of the ambient setpoint as a function of the percentage of infrared radiation emitted by the human body that is reflected by the PNIPAM-based hydrogel composites (20 wt% SiO_2).

addition of silica particles, the percentage of reflected radiation reaches a maximum of 20% (Fig. 1b), in which the application temperature would be 24.7 °C. When different external stimuli such as relative humidity and temperature are applied to the hydrogel composites, the percentage of reflected radiation varies. By changing the relative humidity between 0–90%RH, the reflected radiation varies between 20–30% (Fig. 2b), while corresponding to application temperatures of 24 °C to maintain the thermal comfort. On the other hand, the hydrogel composites reflect between 30–45% of the infrared radiation emitted by the human body when the temperature changes between 20–50 °C (Fig. 4b). In this case, the application temperature would be of 23 °C according to the theoretical models (Fig. 7d). The behavior of the hydrogel composites and their dynamic behavior allow a window of 3 °C in the ambient. Based on the results increasing the percentage of reflected infrared radiation increases the body surface temperature and therefore, in order to maintain thermal comfort, the ambient set point temperature must decrease. Consequently, hydrogel composites capable of modulating the IR emitted by the human body are expected to be used for heating applications, *e.g.* in smart textiles for an outdoor scenario with cold ambient temperatures due to increase of temperature in the microclimate created between the hydrogel and the skin.

E. Conclusions

PNIPAM-based hydrogel composites are successfully prepared by free radical photo-polymerization using NIPAM as monomer, AA as co-monomer, MBA as crosslinker, and TPO as photoinitiator in the presence of submicron-sized spherical SiO_2 particles with a uniform size of 100 nm. The incorporation of SiO_2 particles within the hydrogel network does not significantly modify the physicochemical properties of the final materials. The reflection of infrared radiation depends directly on the particle's content within the hydrogel matrix as well as on the relative humidity and temperature. The percentage of IR reflected (ρ) as a function of SiO_2 content increases with decreasing distance between the silica distributed in the hydrogel according to Bragg's law. The IR reflection as a function of relative humidity depends on both bulk and surface contribution. At low relative humidities, the roughness decreases and the distance between the distributed silica hardly changes, so

that the IR reflection increases. At high relative humidities, although the roughness decreases, the distance between the particles increases and the IR reflection decreases. Increasing the temperature causes the IR reflection to increase as a result of the change of morphology on the surface of the hydrogel composite. As a result, hydrogel composites loaded with 20 wt% SiO_2 at 35 °C and 60%RH reflected 42.5% of the IR radiation in the wavelength range of 5–15 μm. Likewise, the addition of SiO_2 endow the decreasing of the apparent temperature of the hydrogel composite as the material reflects the infrared radiation emitted by the human body. The theoretical models further allow the IR reflection of the hydrogel composite to be analyzed at different levels of interaction as a function of the parameters studied experimentally. Finally, the design of the hydrogel composites and their dynamic behavior allow for a 3 °C window in the ambient set-point temperature. Consequently, the promising results open up the application of this dynamic system in the design of smart textiles capable of modulating the infrared radiation emitted by the human body.

Author contributions

Marjorie Garzón Altamirano: investigation, formal analysis, visualization, writing – original draft. Muluneh Geremew Abebe: investigation, software, visualization. Noémie Hergué: writing – review & editing. Joseph Lejeune: supervision, writing – review & editing. Aurelie Cayla: supervision, writing – review & editing. Christine Campagne: supervision. Bjorn Maes: methodology, writing – review & editing. Eric Devaux: supervision, Funding acquisition. Jérémy Odent: conceptualization, methodology, supervision, writing – review & editing. Jean-Marie Raquez: conceptualization, methodology, supervision, writing – review & editing, funding acquisition.

Conflicts of interest

There are no conflicts to declare.

Acknowledgements

Authors acknowledge support from the European Community (FEDER) in the frame of LCFM-BIOMAT, and H2020-RISE-BIODEST. This work was also supported by Interreg France-Wallonie-Vlaanderen program, under the PHOTONITEX project. Jean-Marie Raquez is a FRS-FNRS senior scientific researcher.

Notes and references

1 N. Bouzida, A. Bendada and X. P. Maldague, Visualization of body thermoregulation by infrared imaging, *Therm. Biol.*, 2009, **34**, 120–126.
2 W. Jung and F. Jazizadeh, Vision-based thermal comfort quantification for HVAC control, *Build. Environ.*, 2018, **142**, 513–523.
3 H. Arens and E. A. Zhang, The skin's role in human thermoregulation and comfort, *Calif. Digit. Libr*, 2006, **15**, 250–260.
4 X. Zhang, S. Yu and B. Xu, Dynamic gating of infrared radiation in a textile, *Science*, 2019, **363**, 619–623.
5 X. Yue, T. Zhang, D. Yang, F. Qiu, Z. Li, G. Wei and Y. Qiao, Ag nanoparticles coated cellulose membrane with high infrared reflection, breathability and antibacterial property for human thermal insulation, *J. Colloid Interface Sci.*, 2019, **535**, 363–370.
6 R. Xiao, C. Hou, W. Yang, Y. Su, Y. Li, Q. Zhang, P. Gao and H. Wang, Infrared-Radiation-Enhanced Nanofiber Membrane for Sky Radiative Cooling of the Human Body, *ACS Appl. Mater. Interfaces*, 2019, **11**, 44673–44681.
7 Y. N. Song, R. J. Ma, L. Xu, H. D. Huang, D. X. Yan, J. Z. Xu, G. J. Zhong, J. Lei and Z. M. Li, Wearable Polyethylene/Polyamide Composite Fabric for Passive Human Body Cooling, *ACS Appl. Mater. Interfaces*, 2018, **10**, 41637–41644.
8 Y. Shabany, *Radiation Heat Trans.*, 2020, **4**, 343–389.
9 C. Liu, A. Y. Song, P. Wu, Y. Peng, C. Zhou, S. Fan, A. Yang, J. Chen, P. B. Catrysse, P.-C. Hsu, C. Zhou, Y. Cui and Y. Liu, Warming up human body by nanoporous metallized polyethylene textile, *Nat. Commun.*, 2017, **8**, 496.
10 E. Pakdel, M. Naebe, L. Sun and X. Wang, Advanced Functional Fibrous Materials for Enhanced Thermoregulating Performance, *ACS Appl. Mater. Interfaces*, 2019, **11**(14), 13039–13057.
11 V. Mizeikis, S. Juodkazis, A. Marcinkevičius, S. Matsuo and H. Misawa, Tailoring and characterization of photonic crystals, *J. Photochem. Photobiol., C*, 2001, **2**, 35–69.
12 R. V. Nair and R. Vijaya, Photonic crystal sensors: an overview, *Prog. Quantum Electron.*, 2010, **34**, 89–134.
13 R. V. Nair and R. Vijaya, Photonic crystal sensors: an overview, *Prog. Quantum Electron.*, 2010, **34**, 89–134.
14 Y. Li, D. X. Wu, J. Y. Hu and S. X. Wang, Novel infrared radiation properties of cotton fabric coated with nano Zn/ZnO particles, *Colloids Surf., A*, 2007, **300**, 140–144.
15 G. Li, F. Wang, P. Liu, C. Gao, Y. Ding, S. Zhang and M. Yang, Antioxidant functionalized silica-coated TiO_2 nanorods to enhance the thermal and photo stability of polypropylene, *Appl. Surf. Sci.*, 2019, **476**, 682–690.
16 K. Panwar, M. Jassal and A. K. Agrawal, TiO_2–SiO_2 Janus particles treated cotton fabric for thermal regulation *Surf, Coatings Technol.*, 2017, **309**, 897–903.
17 K. Panwar, M. Jassal and A. K. Agrawal, TiO2–SiO2 Janus particles with highly enhanced photocatalytic activity, *RSC Adv.*, 2016, **6**, 92754–92764.
18 F. Kundracik, M. Kocifaj, G. Videen and J. Klačka, Effect of charged-particle surface excitations on near-field optics, *Appl. Opt.*, 2015, **54**, 6674.
19 C. Z. Tan, Determination of refractive index of silica glass for infrared wavelengths by IR spectroscopy, *Non-Crystaline Solids*, 1998, **223**, 158–163.
20 Y. Ji, Y. Jiang, H. Liu, L. Wang, D. Liu, C. Jiang, R. Fan and D. Chen, Effects of thermal treatment on infrared optical properties of SiO_2 films on Si Substrates, *Thin Solid Films*, 2013, **545**, 111–115.
21 L. Miao, L. F. Su, S. Tanemura, C. A. J. Fisher, L. L. Zhao, Q. Liang and G. Xu, Cost-effective nanoporous SiO_2-TiO_2

coatings on glass substrates with antireflective and self-cleaning properties, *Appl. Energy*, 2013, **112**, 1198–120523.
22 Y. Li, L. Zhou, G. Liu, L. Chai, Q. Fan and J. Shao, Study on the fabrication of composite photonic crystals with high structural stability by co-sedimentation self-assembly on fabric substrates, *Appl. Surf. Sci.*, 2018, **444**, 145–153.
23 H. L. Lim, Y. Hwang, M. Kar and S. Varghese, Smart hydrogels as functional biomimetic systems, *Biomater. Sci.*, 2014, **2**, 603–6182524.
24 Y. Takeoka, M. Honda, T. Seki, M. Ishii and H. Nakamura, Structural colored liquid membrane without angle dependence, *ACS Appl. Mater. Interfaces*, 2009, **1**, 982–986.
25 A. K. Yetisen, H. Butt, L. R. Volpatti, I. Pavlichenko, M. Humar, S. J. J. Kwok, H. Koo, K. S. Kim, I. Naydenova, A. Khademhosseini, S. K. Hahn and S. H. Yun, Photonic hydrogel sensors, *Biotechnol. Adv.*, 2016, **34**, 250–271.
26 E. P. A. Van Heeswijk, J. J. H. Kloos, N. Grossiord and A. P. H. J. Schenning, Humidity-gated, temperature responsive photonic infrared reflective broadband coatings, *J. Mater. Chem. A*, 2019, **7**, 6113–6119.
27 A. S. Hoffman, Environmentally Sensitive Polymers and Hydrogels, *Biomaterials*, 1991, 42–46.
28 M. Umar, K. Min and S. Kim, Advances in hydrogel photonics and their applications, *APL Photonics*, 2019, **4**, 120901.
29 A. Choe, J. Yeom, R. Shanker, M. P. Kim, S. Kang and H. Ko, Stretchable and wearable colorimetric patches based on thermoresponsive plasmonic microgels embedded in a hydrogel film, *NPG Asia Mater.*, 2018, **10**, 912–922.
30 E. A. Kamoun, E. R. S. Kenawy, T. M. Tamer, M. A. El-Meligy and M. S. Mohy Eldin, Poly(vinyl alcohol)-alginate physically crosslinked hydrogel membranes for wound dressing applications: characterization and bio-evaluation, *Arab. J. Chem.*, 2015, **8**, 38–47.
31 Y. Takeoka and M. Watanabe, Controlled multistructural color of a gel membrane, *Langmuir*, 2003, **19**, 9554–9557.
32 K. Depa, A. Strachota, M. Šlouf and J. Brus, Poly(*N*-isopropylacrylamide)-SiO_2 nanocomposites interpenetrated by starch: stimuli-responsive hydrogels with attractive tensile properties, *Eur. Polym. J.*, 2017, **88**, 349–372.
33 Y. Takeoka and T. Seki, Visualizing conformations of subchains by creating optical wavelength-sized periodically ordered structure in hydrogel, *Langmuir*, 2006, **22**, 10223–10232.
34 G.-R. Lin, Y.-H. Lin, Y.-H. Pai and F.-S. Meng, Si nanorod length dependent surface Raman scattering linewidth broadening and peak shift, *Opt. Express*, 2011, **19**, 597.
35 D. Mergel and M. Jerman, Density and refractive index of thin evaporated films, *Chin. Optics Lett.*, 2010, **8**, 67–72.
36 H. Saito, Y. Takeoka and M. Watanabe, Simple and precision design of porous gel as a visible indicator for ionic species and concentration, *Chem. Commun.*, 2003, 2126–2127.
37 W. Wei, X. Hu, X. Qi, H. Yu, Y. Liu, J. Li, J. Zhang and W. Dong, A novel thermo-responsive hydrogel based on salecan and poly(*N*-isopropylacrylamide): synthesis and characterization, *Colloids Surf., B*, 2015, **125**, 1–11.81.
38 J. Su, Y. Yang, Z. Chen, J. Zhou, X. Liu, Y. Fang and Y. Cui, Preparation and performance of thermosensitive poly(*N*-isopropylacrylamide) hydrogels by frontal photopolymerization, *Polym. Int.*, 2019, **68**, 1673–1680.
39 G. Mayonado, S. M. Mian, V. Robbiano and F. Cacialli, Investigation of The Bragg-Snell Law in Photonic, *Crystals*, 2015, 60–63.
40 *Wrinkled polymer surfaces, strategies, methods and applications*, ed. C. M. González-Henríquez and J. Rodríguez-Hernández, 2019, pp. 320–362.
41 C. Xu, G. T. Stiubianu and A. A. Gorodetsky, Adaptive infrared-reflecting systems inspired by cephalopods, *Science*, 2018, **359**, 1495–1500.
42 C. Xiao, Z. Zhang, X. Chen, X. Song, Y. Cao, C. He and X. Gao, pH- and thermo-responsive poly(*N*-isopropylacrylamide-*co*-acrylic acid derivative) copolymers and hydrogels with LCST dependent on pH and alkyl side groups, *J. Mater. Chem. B*, 2013, **1**, 5578.
43 K. Matsumoto, N. Sakikawa and T. Miyata, Thermo-responsive gels that absorb moisture and ooze water, *Nat. Commun.*, 2018, **9**, 1–7.
44 Y. Tokudome, H. Kuniwaki, K. Suzuki, D. Carboni, G. Poologasundarampillai and M. Takahashi, Thermoresponsive Wrinkles on Hydrogels for Soft Actuators, *Adv. Mater. Interfaces*, 2016, **3**, 1–5.
45 M. Li, B. Bresson, F. Cousin, C. Frétigny and Y. Tran, Submicrometric Films of Surface-Attached Polymer Network with Temperature-Responsive Properties, *Langmuir*, 2015, **31**, 11516–11524.
46 J. Kischkat, S. Peters, B. Gruska, M. Semtsiv, M. Chashnikova, M. Klinkmüller, O. Fedosenko, S. MacHulik, A. Aleksandrova, G. Monastyrskyi, Y. Flores and W. T. Masselink, Mid-infrared optical properties of thin films of aluminum oxide, titanium dioxide, silicon dioxide, aluminum nitride, and silicon nitride, *Appl. Opt.*, 2012, **51**, 6789–6798.
47 Y. Ji, Y. Jiang, H. Liu, L. Wang, D. Liu, C. Jiang, R. Fan and D. Chen, *Thin Solid Films*, 2013, **545**, 111–115.
48 L. V. Rodríguez-de Marcos, J. I. Larruquert, J. A. Méndez and J. A. Aznárez, Self-consistent optical constants of SiO2 and Ta_2O_5 films, *Opt. Mater. Express*, 2016, **6**, 3622.
49 M. G. Abebe, G. Rosolen, E. Khousakoun, J. Odent, J. M. Raquez, S. Desprez and B. Maes, *Phys. Rev. Appl.*, 2020, **14**, 1–13.